Heat Budget of the South-Central Equatorial Pacific in CMIP3 Models

LIU Xiangcui[1,2] and LIU Hailong[*1]

[1]*State Key Laboratory of Numerical Modeling for Atmospheric Sciences and Geophysical Fluid Dynamics,*
Institute of Atmospheric Physics, Chinese Academy of Sciences, Beijing 100029
[2]*Graduate University of the Chinese Academy of Sciences, Beijing* 100049

ABSTRACT

Using data from 17 coupled models and nine sets of corresponding Atmospheric Model Intercomparison Project (AMIP) results, we investigated annual and seasonal variation biases in the upper 50 m of the south-central equatorial Pacific, with a focus on the double-ITCZ bias, and examined the causes for the amplitude biases by using heat budget analysis. The results showed that, in the research region, most of the models simulate SSTs that are higher than or similar to observed. The simulated seasonal phase is close to that observed, but the amplitudes of more than half of the model results are larger than or equal to observations. Heat budget analysis demonstrated that strong shortwave radiation in individual atmospheric models is the main factor that leads to high SST values and that weak southward cold advection is an important mechanism for maintaining a high SST. For seasonal circulation, large surface shortwave radiation amplitudes cause large SST amplitudes.

Key words: double ITCZ, south-central equatorial Pacific, heat budget, annual mean, seasonal variation

1. Introduction

Coupled atmosphere–ocean general circulation models (CGCMs) are a useful tool for investigating climate change. However, CGCMs commonly have some evident biases because of a lack of understanding of the physical processes and interactions among each component in climate systems. The double ITCZ bias (DIB) is one of the remarkable biases found in tropical regions in CGCMs (Mechoso et al., 1995). Figure 1 shows the annual mean precipitation in the tropical Pacific from the Global Precipitation Climatology Project (GPCP) (Adler et al., 2003) and the following three models from phase three of the Coupled Model Intercomparison Project (CMIP3): GFDL-CM20 (Geophysical Fluid Dynamics Laboratory-Climate Model 2.0), NCAR-CCSM3 (National Center for Atmosphere Research-Community Climate System Model 3.0) and IAP-FGOALS (Institute of Atmospheric Physics-Flexible Global Ocean–Atmosphere–Land System model). In the GPCP observational data, precipitation south of the Equator extends southeastward from Papua New Guinea. Rainfall of 6 mm d^{-1} extends as far east as 170°W near 10°S. Compared with observations, the convergence zone simulated by the three coupled models south of the Equator is parallel to the Equator. The contour line for precipitation of 6 mm d^{-1} extends eastward, and there is a

weak rainfall belt that even extends to the coast of Peru. This phenomenon is the so-called DIB in terms of precipitation. In addition to precipitation, the DIB also manifests in SST, sea surface wind, and upper ocean circulation, among others (e.g., Zhang et al., 2007). The annual mean SST shows that, in addition to precipitation biases, all of the models also result in warm SST biases south of the Equator (right panel in Fig. 1). Mechoso et al. (1995) were the first to describe the DIB in coupled models, and though many studies have since investigated the DIB, the bias is still a common problem in coupled models (Lin, 2007; de Szoeke and Xie, 2008; Bellucci et al., 2010; Gent et al., 2011; Zheng et al, 2011).

Many previous studies have concentrated on examining the DIB in the eastern equatorial Pacific, near the coast of Peru. At that location, the bias is believed to be related to a deficient amount of stratus and stratocumulus clouds (Ma et al., 1996) and an insufficient upwelling along the coast (Li et al., 2003). Several recent studies have examined the south-central equatorial Pacific region, where a distinct precipitation bias occurs. The present study also focuses on this region (10°–5°S, 160°E–140°W), which is denoted by the rectangle in Fig. 1.

Zhang et al. (2007) used three directly coupled models to make a preliminary investigation of the DIB in the south-central equatorial Pacific. By analyzing the three models in terms of precipitation, SST, surface winds, thermocline, and ocean currents, a positive feedback mechanism was proposed. The feedback mechanism begins by assuming an ini-

---

[*] Corresponding author: LIU Hailong
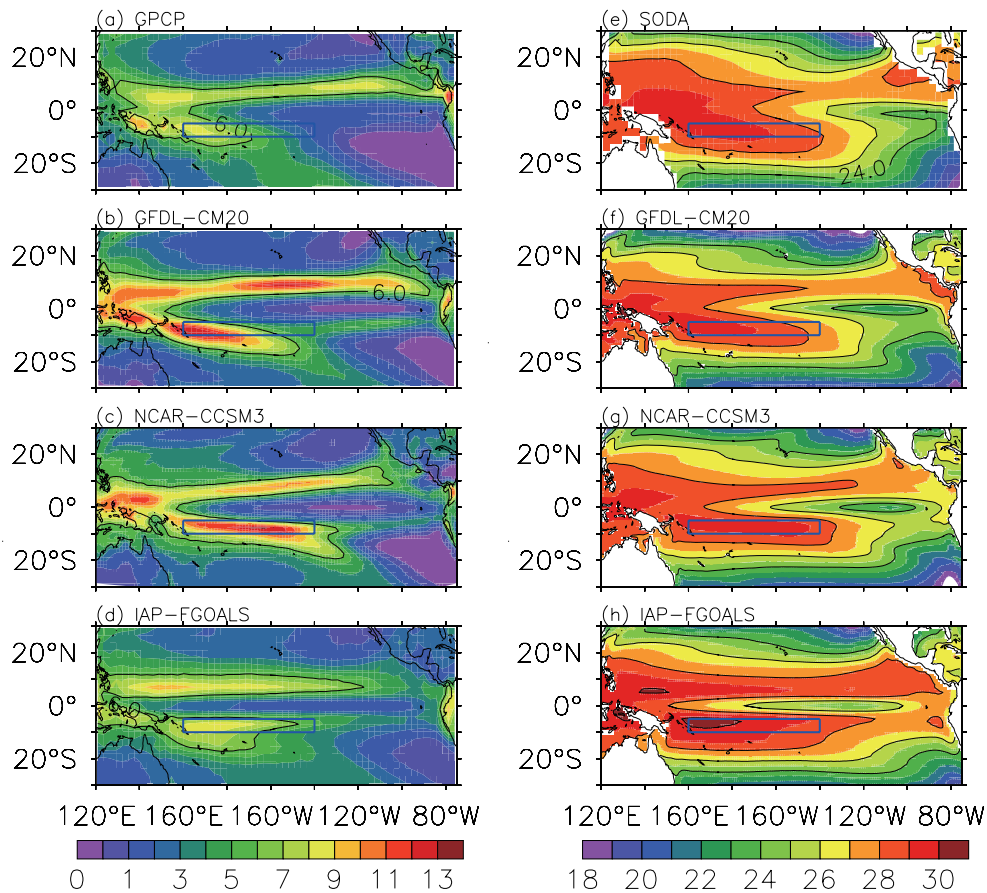   Email: lhl@lasg.iap.ac.cn

Fig. 1. (Left) annual mean precipitation (mm d^{-1}) of (a) GPCP and three coupled CMIP3-20C3M models (b) GFDL-CM20, (c) NCAR-CCSM3, and (d) IAP-FGOALS. (Right) the same as the left, but for the SST (°C) using SODA data as the observational data. The blue rectangle represents the research region (10°–5°S , 160°E–140°W).

tially positive precipitation perturbation in the models. The atmospheric latent heating associated with the precipitation anomaly results in surface winds that converge toward the precipitation region, leading to a negative surface wind curl anomaly south of the precipitation region. A thermocline ridge occurs as a result of Ekman pumping. Next, an eastward SECC (South Equatorial Counter Current) anomaly is formed north of the ridge. The SECC transfers warm water eastward, which causes a positive SST anomaly to form at the eastern edge of the initial precipitation anomaly. This can move the initial precipitation perturbation further eastward, forming a positive feedback mechanism. Zhang and Song (2010) suggested that the DIB in CCSM3 can be effectively alleviated by revising the convective closing assumption in the convective parameterization scheme. In CCSM3, a slab ocean model is coupled with the atmospheric component using a revised Zhang–McFarlane (ZM) convection scheme. The result shows that the simulated SST is very sensitive to the prescribed ocean heat transport required in the slab ocean model. In revised coupled models, ocean heat transport is largely responsible for the reduction of SST bias in the southern ITCZ region. Liu et al. (2012) also investigated the initial development of the DIB in CCSM3. Their study also showed that the warming bias is caused by dynamic heat transport

by ocean currents. Not only the zonal-current advection, but also the meridional-current advection, plays an important role in the development of the SST anomaly in the south-central equatorial Pacific.

On the one hand, the above research shows that the SST bias plays an important role in the development of the DIB. On the other hand, some research has found that the relationship between the SST and convection in coupled models is much closer than in observations (e.g., Lin, 2007). Table 1 shows the annual mean SST and precipitation from GPCP/Simple Ocean Data Assimilation (SODA) and 17 CMIP3 directly-coupled models in the south-central equatorial Pacific. Except for MIROC-32H, MIROC-32M and UKMO-HadGEM1, the models overestimate the precipitation in the south-central equatorial Pacific. Additionally, the role of ocean currents should not be ignored. This includes the zonal currents initially proposed by Zhang et al. (2007) and the meridional currents. However, these previous studies mainly focused on a few individual models, making it difficult to reach a common conclusion because of the large differences among models. It is thus necessary to analyze results from multiple models. A thorough understanding of the SST variations in the south-central equatorial Pacific will increase the understanding of the DIB generation mechanism.

Table 1. List of the 17 CMIP3 models used in this study. The observational data are from GPCP and SODA. The annual mean SST and precipitation in the south-central equatorial Pacific are also shown. The values after the positive/negative symbols correspond to seasonal standard deviations.

	Model center (or data name)	Model name	Reference	Precipitation (mm d^{-1})	SST (°C)
0	GPCP/SODA	–	Alder et al. (2003); Carton and Giese (2008)	5.3±1.4	28.8±0.3
1	Bjerknes Centre for Climate Research (Norway)	BCCR-BCM2	Xu et al. (2005)	5.4±0.8	27.3±0.2
2	Centre National de Recherches Météorologiques (France)	CNRM-CM3	Salas-Mélia et al. (2005)	6.3±0.9	27.0±0.1
3	Commonwealth Scientific and Industrial Research Organisation Atmospheric Research (Australia)	CSIRO-Mk3.0	Godon et al. (2002)	6.8±0.8	28.6±0.2
4	CSIRO Atmospheric Research (Australia)	CSIRO-Mk3.5	Gordon et al. (2002)	7.8±0.9	30.0±0.3
5	Geophysical Fluid Dynamics Laboratory (USA)	GFDL-CM2.0	Delworth et al. (2006)	7.0±1.4	28.6±0.4
6	National Aeronautics Space Administration Goddard Institute for Space Studies (USA)	GISS-AOM	Russell et al. (1995)	6.7±1.2	28.3±0.5
7	NASA Goddard Institute for Space Studies (USA)	GISS-MEH	Schmidt et al. (2006)	6.3±1.7	28.4±0.3
8	Institute of Atmospheric Physics (China)	IAP-FGOALS	Yu et al. (2004)	7.0±1.4	29.4±0.5
9	National Institute of Geophysics and Volcanology (Italy)	INGV-ECHAM4	Gualdi et al. (2008)	7.4±1.1	28.7±0.3
10	Institute Pierre Simon Laplace (France)	IPSL-CM4	Marti et al. (2005)	8.6±0.9	29.8±0.5
11	Max Planck Institute for Meteorology (German)	MPI-ECHAM5	Jungclaus et al. (2006)	6.7±0.9	29.3±0.3
12	Center for Climate System Research, National Institute (Japan)	MIROC-32H	Hasumi and Emori (2004)	4.9±1.9	27.6±0.9
13	Center for Climate System Research, National Institute (Japan)	MIROC-32M	Hasumi and Emori (2004)	4.6±1.3	27.4±0.6
14	National Center for Atmospheric Research (USA)	NCAR-CCSM3	Collins et al. (2006)	10.0±1.1	29.2±0.5
15	National Center for Atmospheric Research (USA)	NCAR-PCM1	Meehl et al. (2004)	6.4±1.4	28.6±0.8
16	Hadley Centre for Climate Prediction and Research, Met Office (UK)	UKMO-HadCM3	Gordon et al. (2000)	7.8±0.4	29.7±0.2
17	Hadley Centre for Climate Prediction and Research, Met Office (UK)	UKMO-HadGEM1	Johns et al. (2006)	4.4±1.3	27.5±0.3

In the present reported study, results from 17 directly-coupled models from CMIP3 were analyzed. The main processes that control SST variations in the south-central equatorial Pacific were investigated by diagnosing the heat budget of the upper 50 m of the ocean. Comparisons were made between the models and the observations. The remainder of the paper is organized as follows. Section 2 describes the data and method used to calculate the heat budget. Section 3 analyzes the annual and seasonal variations of SST in the south-central equatorial Pacific. Section 4 presents the heat budget of upper 50 m of the regional ocean. Section 5 analyzes dynamic ocean processes, and the final section summarizes the major findings.

2. Data and method

2.1. *Model data and their uncertainty*

We used 17 sets of directly-coupled model results from CMIP3 under the 20C3M scenario, not including the following six coupled models with flux-correction: BCC-CM1, CCCMA-CGCM3, CCCMA-CGCM3T63, MIUB-ECHOG, MRI-CGCM2 and INM-CM3.0. Table 1 lists the model names, acronyms and references. Only 14 of the coupled models were used to calculate the heat budget because some variables were unknown in the other three models (GFDL-CM2.0, GISS-MEH and INGV-ECHAM4). The analysis car-

ried out in the present paper is based on the 50-yr (1950–99) average of the CMIP3 and six corresponding AMIP runs (1979–99), which were used to investigate the origin of the biases.

The uncertainty of the model results was estimated using the following formula:

$$f = \frac{ks}{\sqrt{n}} \; .$$

Where

$$s = \sqrt{\frac{\sum\limits_{n} (x - \bar{x})^2}{n - 1}}$$

is the estimated standard deviation, in which $\bar{x} = \frac{1}{n} \sum\limits_{n} x$ is the mean and n is the number of measurements; and k is the coverage factor. Since the sample size was small and the population standard deviation was unknown, the Students t distribution was chosen. Therefore, $k = 2.262$ at a confidence level of 95%. The multi-model ensemble (MME) and the uncertainties are given in each figure using blue circles and blue vertical lines, respectively, we use the values to measure the spread among the models. However, it should be noted that, because the truth is unknown, the deviations around the ensemble mean may have resulted in an underestimation of the error variance.

2.2. *Observational datasets*

Datasets of surface fluxes can usually be grouped into three categories: voluntary observing ship (VOS)-based, satellite-derived, and blended. However, each of these three types has its own problems. For VOS-based datasets, the biases are attributed to the sampling and variable corrections (Kent and Berry, 2005; Gulev et al., 2007). For satellite-derived datasets, the biases mainly come from the uncertainty of retrievals. For instance, the surface shortwave radiation data in the International Satellite Cloud Climatology Project (ISCCP) (Zhang et al, 2004) dataset are overestimated by 5%–10% in the tropical region (e.g., Large and Yeager, 2008; Liu et al., 2010). For the blended products, although the balance is normally achieved, the problem of physical justification of variable corrections still remains.

The selection of datasets in the present study was based on Liu et al. (2010), who contrasted the mixed-layer heat budget in the south-central equatorial Pacific with several objectively-analyzed surface energy fluxes and ocean assimilation products. Their results showed that the adjusted National Ocean Center surface heat fluxes dataset version 1.1 (NOC1a) (Grist and Josey, 2003) can describe the real conditions in the south-central equatorial Pacific well compared with buoy data. Therefore, the climatological monthly mean ocean surface heat fluxes from NOC1a (1980–93) were selected as the observational reference in the present study. In addition, latent heat flux and sensible heat flux data from the Objectively Analyzed Air–Sea Fluxes (OAFlux) project (Yu and Weller, 2007), which is considered to perform fairly well globally (Yu and Weller, 2007; Song and Yu, 2012), were used to evaluate the latent and sensible fluxes in the models.

Liu et al. (2010) also concluded that four ocean reanalysis datasets they evaluated are all suitable to describe the surface net flux and horizontal heat transport over the region of the DIB. Since the SODA (Carton and Giese, 2008) dataset has both a longer duration (1958–2007) and higher horizontal resolution ($0.5° \times 0.5°$) than the other two products, the monthly mean temperature, three-dimensional velocity and net surface heat flux from SODA between 1993 and 2004 were used to compute the climatology of the heat budget over the south-central equatorial Pacific in the present study.

2.3. *Method for calculating ocean surface heat flux*

To evaluate temperature variations over the south-central equatorial Pacific in the coupled models, we analyze the heat budget for the upper 50 m of the ocean in the study domain using monthly-averaged data. According to Liu et al. (2010), the thermodynamic equation is written as follows:

$$\rho_0 c_p h \frac{\partial \langle T \rangle}{\partial t} = -\rho_0 c_p h \left\langle \frac{\partial uT}{\partial x} + \frac{\partial vT}{\partial y} \right\rangle + Q_0 - Q_{\text{pen}} + R \,, \tag{1}$$

where u, v and T are the zonal current, meridional current and temperature, respectively; h is the mixed-layer depth (fixed to 50 m in the present study); ρ_0 ($= 1026$ kg m^{-3}) is the reference oceanic density; $c_p [= 3996$ J (kg K)$^{-1}]$ is the specific heat of seawater; Q_0 is the net downward surface heat flux;

Q_{pen} is the shortwave radiation that penetrates the bottom of the mixed layer; and R is the sum of additional terms representing vertical advection and all subgrid-scale processes such as horizontal diffusion, vertical diffusion at the bottom of the mixed layer and convection. The R term includes the entrainment of cold water into the mixed layer from below. Brackets $<>$ denote a vertical average over the upper 50 m of ocean water. From left to right, the five terms represent temperature tendency, horizontal advection, net sea surface heat flux, shortwave penetration and residual.

The method used for computing the horizontal temperature advection term was from Lee et al. (2004). The volume-averaged temperature of the target domain is used as the reference temperature in their formulation. The interface temperature advections are represented by the interface current multiplied by the difference between the interface and reference temperature. The zonal (meridional) advection is the difference between two zonal (meridional) interfaces. This method sufficiently embodies the effects of external processes on the domain-averaged temperature.

Shortwave penetration was estimated using the following formula:

$$Q_{\text{pen}}(z) = Q_{\text{sw}} \times [\alpha e^{-z/z_1} + (1 - \alpha)e^{-z/z_2}] \,. \tag{2}$$

In our study, downward net surface fluxes are positive. In this equation, the Q_{sw} is the net surface shortwave radiation. The two terms in the right side represent the percentage of solar radiation in the infrared band and the ultraviolet and visible band which penetrated below a certain depth. The e is the standard of the natural exponential function and the z in the Eq. (2) represents the depth of solar radiation penetration, which was fixed at 50 m in the present study. We used the values $\alpha = 0.58, z_1 = 0.35$ m, and $z_2 = 23$ m, according to Rosati and Miyakoda (1988).

3. Annual mean temperature and its seasonal variations

The annual mean temperature and precipitation over the south-central equatorial Pacific are shown in Table 1. Most of the models (14 out of 17) simulate more precipitation than observed. Although some models simulate lower temperatures than observed, they also simulate higher precipitation. This characteristic is related to the threshold temperature in the convection parameterization that triggers rainfall.

Figure 2 shows the seasonal cycle of SST and its anomaly (deducted annual mean). Observations show that the seasonal SST cycle peaks in April and reaches a minimum in August. The standard deviation of seasonal variations is 0.3°C. Most of the models can simulate the phases of this annual cycle well, except for NCAR–PCM1, which shows an SST peak in January. Therefore, we do not discuss this model in the following parts of the paper. There are two main differences in the SST seasonal variations between the simulations and observations. First, there is a large difference in the annual mean values, as evident in Table 1, which has a maximum
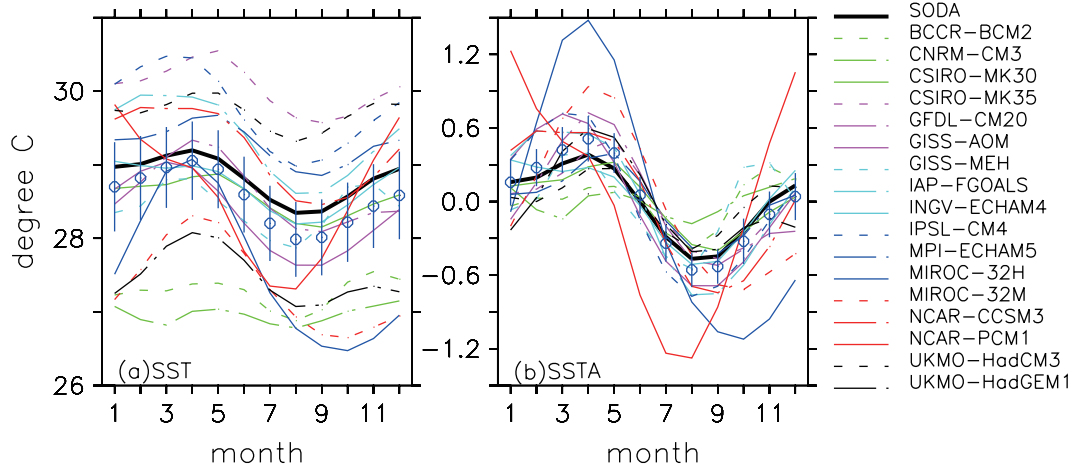
Fig. 2. Seasonal SST and SST anomaly in the south-central equatorial Pacific from SODA and the 17 CMIP3 models. The blue circles and blue vertical lines are the multi-model ensemble and uncertainties, respectively. Units: °C.

of 30°C and minimum of 27°C. Second, most of the models simulate larger seasonal variation amplitudes than observed. The seasonal variation amplitude is approximately 0.3°C for observations, but exceeds 0.5°C in more than half of the models. Because of these discrepancies, one may question what process causes the difference in annual mean temperature and why models simulate a larger SST seasonal variation than observed. Determining the answers to these questions will allow for an increased understanding of the DIB.

Because the model results used are equilibrium-state data, we also compared the model results with the AMIP results, as described below, to help understand the annual mean temperature bias.

4. Heat budget of the upper 50 m of the ocean

To investigate the processes leading to the SST variations, we calculated the five terms (temperature tendency, horizon-tal temperature advection, net surface heat flux, shortwave penetration, and residuals) in the heat budget equation for the upper 50 m of the ocean using the method presented in section 2. By comparing the temperature tendency and the other four terms, it is possible to determine the main process that induces biases in the SST seasonal variation.

4.1. *Annual mean*

Table 2 shows the annual mean values of the five terms of the heat budget. The temperature tendency differs by an order of magnitude from the other terms, which implies that the models have reached equilibrium state. The observation shows that the 14 W m^{-2} sea surface heat flux is primarily balanced by horizontal zonal advection (-10 W m^{-2}) and solar radiation penetration (-10 W m^{-2}). The residual term is the warming effect with a value of 6 W m^{-2}.

Simulated surface heating also contributes to heating, and shows great differences from observations. Simulated surface

Table 2. The heat budget and seasonal standard deviation from SODA and the 17 CMIP3 models in the south-central equatorial Pacific (units: W m^{-2}). The metrics after $+/-$ are the standard deviation of the monthly climatology of each variable.

No.	Tendency	Surface HF	Horizontal Advection	SW Penetration	Residual
0	0 ± 11	14 ± 22	-10 ± 3	-10 ± 1	6 ± 10
1	0 ± 9	0 ± 13	3 ± 5	-10 ± 1	7 ± 9
2	0 ± 6	18 ± 10	1 ± 2	-9 ± 1	-10 ± 6
3	0 ± 10	7 ± 21	-7 ± 8	-9 ± 1	9 ± 5
4	0 ± 13	7 ± 19	-5 ± 6	-9 ± 1	7 ± 3
5	—	—	—	—	—
6	0 ± 19	12 ± 30	3 ± 2	-11 ± 1	-4 ± 9
7	—	—	—	—	—
8	0 ± 19	9 ± 24	-1 ± 3	-10 ± 1	2 ± 4
9	—	—	—	—	—
10	0 ± 21	7 ± 29	6 ± 7	-11 ± 1	-2 ± 4
11	0 ± 11	10 ± 22	-3 ± 12	-11 ± 1	4 ± 6
12	0 ± 30	23 ± 44	-19 ± 10	-11 ± 1	7 ± 13
13	0 ± 22	16 ± 37	-17 ± 13	-10 ± 1	11 ± 10
14	0 ± 21	31 ± 26	-1 ± 5	-10 ± 1	-20 ± 3
15	0 ± 36	11 ± 32	2 ± 38	-11 ± 1	-2 ± 69
16	0 ± 10	10 ± 15	-5 ± 4	-11 ± 1	6 ± 6
17	0 ± 14	18 ± 25	-23 ± 12	-12 ± 1	17 ± 5
Mean	0	12.3	-1.5	-10.3	-0.5

heating reaches a maximum in NCAR-CCSM3 (31 W m^{-2}) and a minimum in BCCR-BCM2 (0 W m^{-2}). The surface heat flux is composed of four items: net surface shortwave radiation, net surface longwave radiation, surface latent heat flux, and surface sensible heat flux. The annual mean values of the four items are shown in Table 3, along with the observational values from both NOC1a and OAFlux. The NCAR-CCSM3 model has a larger surface heat flux because less latent heat flux is released, whereas CSIRO-MK3.5 has a weak surface heat flux because it has weak shortwave radiation. Most of the models underestimate the sea surface heat flux, which is coincident with high temperatures and weak wind stresses.

The differences in the simulated horizontal temperature advection are much larger than in the surface heat flux; some models result in warm advection, and other models result in cold advection. Cold advection is prominent in MIROC-32H, MIROC-32M and UKMO-HadGEM1, which balance the overestimated net surface heat flux. Other models simulate weak cold advection or warm advection, contributing to a decrease in the cooling effect of horizontal advection. This is one of the potential processes that can cause a high SST.

The differences in shortwave radiation penetration between the models and observations are relatively small (approximately -10 W m^{-2}) and contribute to cooling. In this term, small differences are because of the great effect of depth but weak role of shortwave radiation. Based on Eq. (2), the 20 W m^{-2} differences in shortwave radiation lead to only a 1 W m^{-2} difference in shortwave penetration.

Because of the feedback among the SST, clouds and wind, the SST can affect the surface heat flux, based on its

Table 3. The annual mean and seasonal standard deviation of the four terms in the heat budget from NOCS1a and the 17 CMIP3 models in the south-central equatorial Pacific (units: W m^{-2}). The metrics after $+/-$ are the standard deviation of the monthly climatology of each variable.

No.	Shortwave	Latent	Longwave	Sensible
0	211 ± 21	$-138 \pm 8 /$ -128 ± 5	-52 ± 2	$-7 \pm 1 /$ -8 ± 1
1	201 ± 25	-144 ± 16	-46 ± 6	-11 ± 2
2	191 ± 15	-133 ± 10	-32 ± 3	-8 ± 1
3	189 ± 19	-118 ± 5	-48 ± 1	-16 ± 1
4	189 ± 17	-128 ± 10	-43 ± 2	-11 ± 1
5	—	—	—	—
6	222 ± 23	-133 ± 7	-44 ± 1	-33 ± 2
7	—	—	—	—
8	211 ± 22	-139 ± 8	-48 ± 2	-15 ± 0
9	—	—	—	—
10	224 ± 26	-131 ± 9	-69 ± 1	-17 ± 1
11	233 ± 25	-157 ± 9	-53 ± 3	-13 ± 1
12	226 ± 25	-136 ± 26	-59 ± 2	-8 ± 1
13	211 ± 22	-129 ± 18	-57 ± 2	-9 ± 1
14	203 ± 19	-111 ± 14	-49 ± 1	-12 ± 1
15	228 ± 22	-149 ± 27	-52 ± 2	-16 ± 2
16	229 ± 20	-154 ± 10	-55 ± 1	-10 ± 0
17	256 ± 29	-162 ± 9	-66 ± 3	-10 ± 1
Mean	215	-137	-53	-13

Table 4. The annual mean and seasonal standard deviation (units: W m^{-2}) of the net surface heat flux and its four terms, from NOCS1a and 9 AMIP models in the south-central equatorial Pacific. The metrics after $+/-$ are the standard deviation of the monthly climatology of each variable.

No.	Net	Shortwave	Latent	Longwave	Sensible
2	12 ± 13	207 ± 17	-157 ± 10	-33 ± 1	-5 ± 1
8	—	204 ± 18	-143 ± 14	—	-13 ± 1
10	22 ± 30	240 ± 27	-130 ± 10	-72 ± 2	-16 ± 1
11	8 ± 20	229 ± 16	-159 ± 14	-52 ± 2	-10 ± 1
12	20 ± 39	221 ± 25	-133 ± 20	-59 ± 2	-9 ± 1
13	5 ± 36	207 ± 21	-138 ± 20	-55 ± 1	-9 ± 1
14	39 ± 34	224 ± 21	-123 ± 18	-53 ± 1	-9 ± 1
15	—	239 ± 24	-126 ± 14	—	-12 ± 1
17	—	271 ± 22	-162 ± 13	—	-9 ± 1
Mean	18.8	227	-136	-58.2	-12

effect on the amount of clouds and the wind speed in the coupled model. Air–sea feedback in coupled models can reduce the surface heat flux bias. Therefore, the heat flux bias in the corresponding AMIP results is investigated in general atmospheric models (Table 4). Most of the AMIP models overestimate the net surface heat flux, primarily because of strong shortwave radiation. As a result, the large surface heat flux found in individual atmospheric models plays an important role in the high temperature in coupled models.

As shown above, the analysis based on equilibrium states and individual atmospheric models indicates that there are two causes of high temperatures: the overestimation of the surface heat flux in the atmospheric models, especially the surface shortwave radiation, and the weak cooling advection in coupled models. The ensemble mean of the net surface heat flux of the five atmospheric models is 18.8 W m^{-2} (Table 4). It is approximately 6–7 W m^{-2} larger than observed. The mean bias of the horizontal temperature transport is around 8.5 W m^{-2} (Table 2): 0.8 W m^{-2} for the zonal direction and 7.7 W m^{-2} for the meridional direction (Table 5). However, such kinds of biases cannot be found in the standalone oceanic model. Therefore, although the bias in the temperature advection seems to be larger than the bias in the net surface heat flux, we believe that it is the latter that triggers the development of the biases in the other terms in this region.

4.2. *Seasonal variation*

Based on the SST standard deviation in Table 1, it is apparent that models simulate large seasonal amplitudes. To investigate the reason for such large amplitudes, the seasonal variation of a surface heat budget is analyzed (Fig. 3). In the observations, the temperature tendency indicates a warming from January to April and September to December and a cooling from May to August. This causes a temperature maximum in April and a temperature minimum in September, with amplitude as high as 11 W m^{-2}. Models can simulate the same seasonal variation phase well. However, more than half of the models simulate much larger amplitude for warming and cooling than observed (Table 2). If we com-

Table 5. The annual mean regional-averaged zonal advection in the south-central equatorial Pacific and the corresponding east/west boundary advection, meridional advection, and north/south boundary advection.

No.	Zonal advection	Western boundary	Eastern boundary	Meridional advection	Southern boundary	Northern boundary
0	−6	1	7	−4	1	5
1	0	1	1	3	3	0
2	−2	−1	1	3	3	0
3	−4	1	5	−3	2	5
4	−7	0	7	2	4	2
5	—	—	—	—	—	—
6	1	2	1	2	3	1
7	—	—	—	—	—	—
8	−5	1	6	4	4	0
9	—	—	—	—	—	—
10	−3	0	3	9	7	−2
11	−4	1	5	1	7	6
12	−17	−5	12	−2	1	3
13	−11	−4	7	−6	2	8
14	−5	−1	4	4	4	0
15	−24	−18	6	26	20	−6
16	−7	2	9	2	4	2
17	−10	3	13	−13	2	15
Mean	−5.2	0.5	5.7	3.7	5	1.3

pare observations and the MME plus uncertainties, we find that the differences between the models and observations are large in winter and summer but small in the transition seasons (Fig. 3a). The amplitudes of three models (MIROC-32H, MIROC-32M and UKMO-HadGEM1), are much larger than observed, particularly for MIROC-32H and MIROC-32M, which have amplitudes greater than 20 W m^{-2}.

To understand the seasonal variation of the SST, the seasonal variation of the net surface heat flux, horizontal temperature advection, shortwave penetration and residual are investigated. The standard deviations of these four items are shown in Table 2. Among the four items, the seasonal variation of net surface heat flux is the most evident, making it the main factor that contributes to the SST variation. For the net surface heat flux, models can simulate seasonal phases that are relatively similar to observations, but with larger amplitude. Large uncertainties can be found especially in the summer and winter seasons. The observed amplitude of the seasonal variation of the net surface heat flux is 22 W m^{-2}, whereas models have amplitudes as large as 44 W m^{-2} (particularly MIROC-32H and MIROC-32M). Therefore, the bias in surface heat flux is a major factor that leads to large SST amplitude.

The seasonal horizontal temperature advection variation, with amplitude of 3 W m^{-2}, is very weak in comparison to the net surface heat flux. The observation shows that cold advection occurs throughout the year and is stronger in boreal winter and weaker in summer. The horizontal temperature advection shows an opposite phase compared to the net surface heat flux, which contributes to reducing the effects of seasonal variations in the SST. Three models (MIROC-32H, MIROC-32M and UKMO-HadGEM1) show overly strong cold advection for the entire year. The annual mean horizontal temperature advections simulated by the other mod-

els show weak cooling effects or warm advection. The other models, except for NCAR-PCM1, appear in-phase with observations, and have their strongest warm (weakest cold) advection in boreal summer (winter). However, the amplitudes of the simulated seasonal variations are large compared to those observed. This suggests that the effect of horizontal temperature advection also contributes to the reduction in SST amplitude.

The residuals also show seasonal variations with amplitudes of approximate 10 W m^{-2}. These variations are larger than the horizontal temperature advection and are stronger in summer and weaker in winter. The residual terms simulated by MIROC-32H, MIROC-32M, and UKMO-HadGEM1 agree with observations, whereas the amplitudes simulated by the other models tend to increase the amplitude of SST and indicate strong heating in winter and weak heating in summer. Shortwave penetration almost remains constant at −10 W m^{-2} for the entire year, making it an unlikely contributor to seasonal SST variations.

According to the above analysis, the net surface heat flux is the leading process that affects the seasonal SST variations. It is thus necessary to evaluate the four components of the net surface heat flux: net surface shortwave radiation, net surface longwave radiation, the surface latent heat flux, and the surface sensible heat flux. Their area-averaged values are shown in Fig. 4, and their mean and standard deviations are shown in Table 3. The shortwave radiation and latent heat flux are the two most important terms and have large seasonal variations. The simulated seasonal variabilities of shortwave radiation are in-phase with observations, enhancing the seasonal SST cycle. The MIROC-32H, MIROC-32M and UKMO-HadGEM1 models simulate extremely large amplitudes, whereas the other models simulate weak amplitudes (resulting in a relatively obvious DIB). The reduction
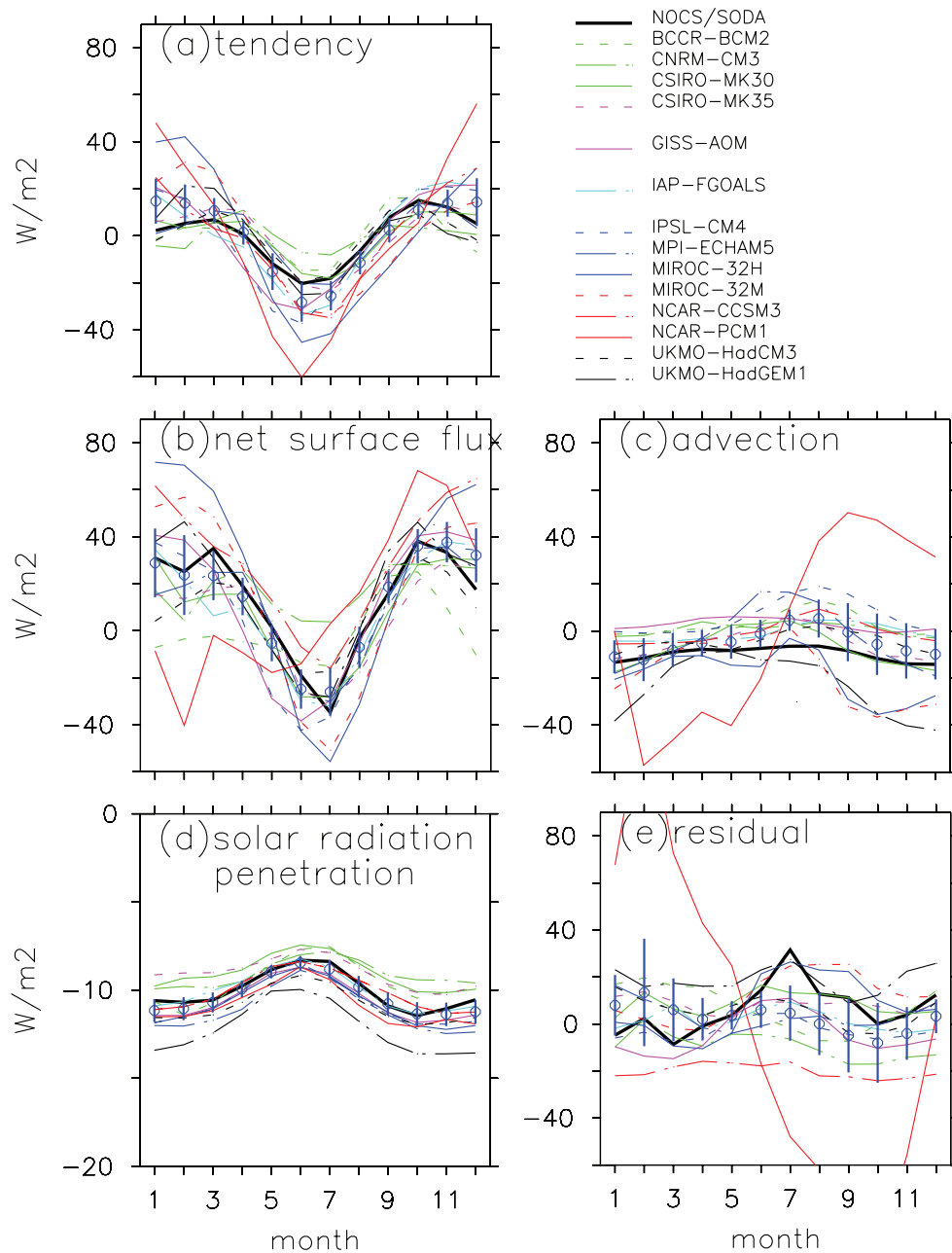
Fig. 3. The climate seasonal temperature tendency, net surface heat flux, horizontal temperature advection, shortwave penetration and residual for SODA/NOCS1a and the 17 CMIP3 models in the south-central equatorial Pacific. The blue circles and blue vertical lines are the multi-model ensemble and uncertainties, respectively. Units: W m^{-2}.

in shortwave radiation is caused by excessive clouds in the research domain. The latent heat flux situation is more complicated. Because the models have different phases with the observation, the effects of the latent heat on the seasonal variation are different. The latent heat causes large SST amplitudes in some of the models (e.g., MIROC-32H and MIROC-32M), and small amplitudes in other models (e.g., BCCR-BCM2 and CNRM-CM3). Some other models (e.g., IAP-FGOALS) can proficiently simulate the seasonal variation of the latent heat flux.

We also investigate the seasonal variations of the surface heat flux in AMIP results over the research domain. Figure 5 shows the four components from AMIP. Their mean values and standard deviations are listed in Table 4. There are only nine models to be analyzed: four of them simulate larger seasonal variations than observed; two are close to observations; and the other three are not evaluated because of a lack of longwave radiation. Figure 5 shows that, although the average values of shortwave radiation are generally larger than observed, the amplitudes are not significantly greater than
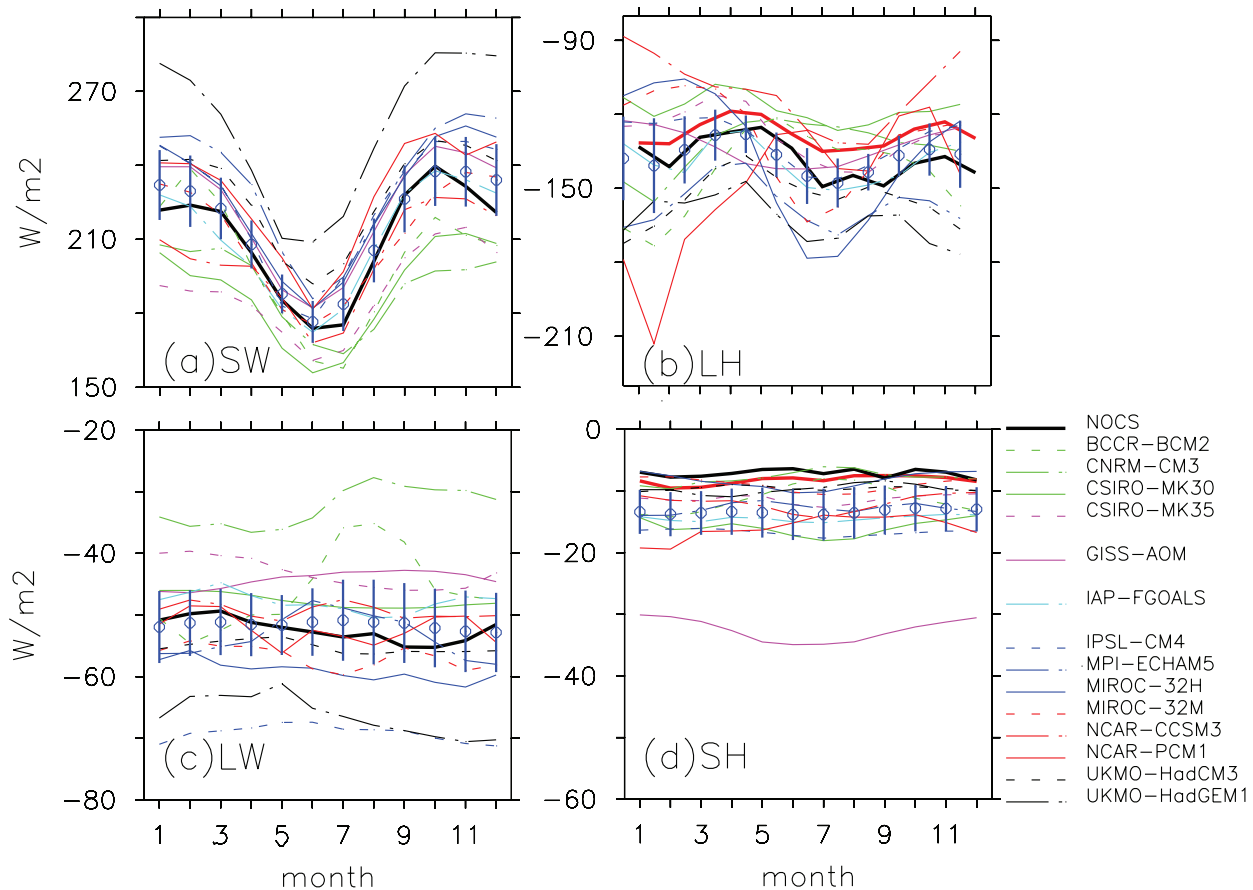
Fig. 4. The climate seasonal shortwave radiation, latent heat flux, longwave radiation and sensible heat flux from NOCS1a and the 17 CMIP3 models in the south-central equatorial Pacific. The blue circles and blue vertical lines are the multi-model ensemble and uncertainties, respectively. Units: W m^{-2}.

those of the observations. The seasonal variations of the latent heat flux that are simulated by AMIP experiments are all greater than observed and show consistent phases. The seasonal variation of the latent heat flux thus leads to the large variation in net surface heat flux in AMIP models. Therefore, the differences between the stand-alone atmospheric models and the coupled models indicate that the air–sea interaction strengthens the seasonal variation of shortwave radiation through the interaction between temperature and cloud.

Although horizontal temperature advection contributes to weakening the seasonal variations of the SST, according to the analysis of the annual mean state, the effect of horizontal temperature advection on the warming bias cannot be ignored. Therefore, it is necessary to further analyze why the horizontal temperature advection modifies the warming bias. Figure 6 shows the seasonal variations of the zonal and meridional horizontal temperature advection. According to observations, the zonal and meridional horizontal temperature advections are cooling effects with similar magnitudes. The zonal advection is mainly a result of the westward transport of cold water in the eastern Pacific by the South Equatorial Current (SEC), and the meridional advection is mainly a result of the southward transport of equatorial cold wa-

ter by the surface Ekman current. The seasonal variation of zonal advection is appropriately the same as the meridional seasonal variation, and both variations have small amplitude. The phase of the zonal advection seasonal cycle is small in winter and large in summer, which is opposite to the meridional phase. There are two main differences between the models and observations: the models simulate weaker cold advection than in the observations for both zonal and meridional advection, and the simulated seasonal meridional advection variation is larger than in the observations. Most experimental results also show a weak cold advection compared to that in observations.

Following Lee et al. (2004), the equation that calculates the horizontal temperature advection can be written as follows:

$$T_{vx} = u_W(T_W - T_{ref}) - u_E(T_E - T_{ref}),$$
$$T_{vy} = u_S(T_S - T_{ref}) - u_N(T_N - T_{ref}),$$

where the subscripts "W", "E", "S" and "N" represent west, east, south and north, respectively. The variables using these subscripts represent the corresponding boundaries of the research domain. The variable T_{ref} represents the domain-
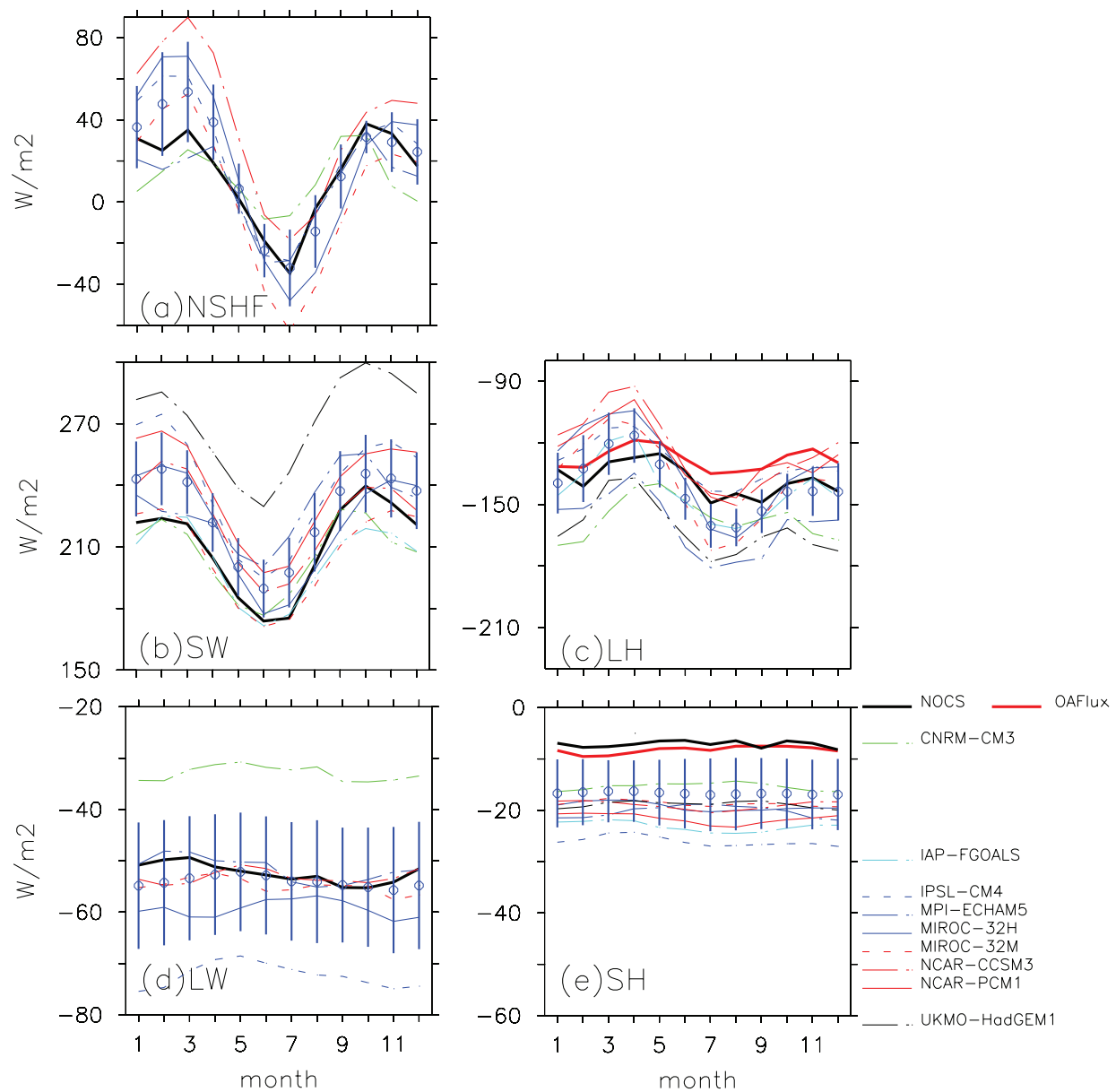
Fig. 5. The climatological seasonal variation in (a) net surface heat flux, (b) shortwave radiation, (c) latent heat flux, (d) longwave radiation, and (e) sensible heat flux of NOCS1a and 9 AMIP models in the south-central equatorial Pacific (units: W m^{-2}). For longwave radiation, there are no data from IAP-FGOALS, NCAR-PCM1 and UKMO-HadGEM1. The blue circles and blue vertical lines are the multi-model ensemble and uncertainties, respectively.

averaged temperature. According to the equation, the annual mean values of advection of the four boundaries are shown in Table 4. Combined with the boundary velocity and temperature gradients (not shown), the observed west boundary zonal advection consists of eastward warm transport by the South Equatorial Counter Current (SECC), and the observed east boundary zonal advection consists of westward cold transport by the SEC. The magnitudes of the two advections are 1 W m^{-2} and 7 W m^{-2}, respectively. Therefore, advection by SEC in the east boundary plays a dominant cooling role.

While the warm water south of the Equator extends too far eastward in coupled models, it reduces the temperature

gradient in the east boundary. Furthermore, the models tend to have weak SECs. This causes the advection in the east boundary to become weak, which weakens the zonal cooling advection process.

As observed, meridional advection is mainly the result of cold advection by the southward Ekman current in the north boundary, which transports the upwelling cold water southward, while in the south boundary, it shows weak warm advection. In most of the coupled models, the southward cold advection is weak, and the warm advection in the south boundary is strong. These two changes make the meridional advections in coupled models mainly warm advections.
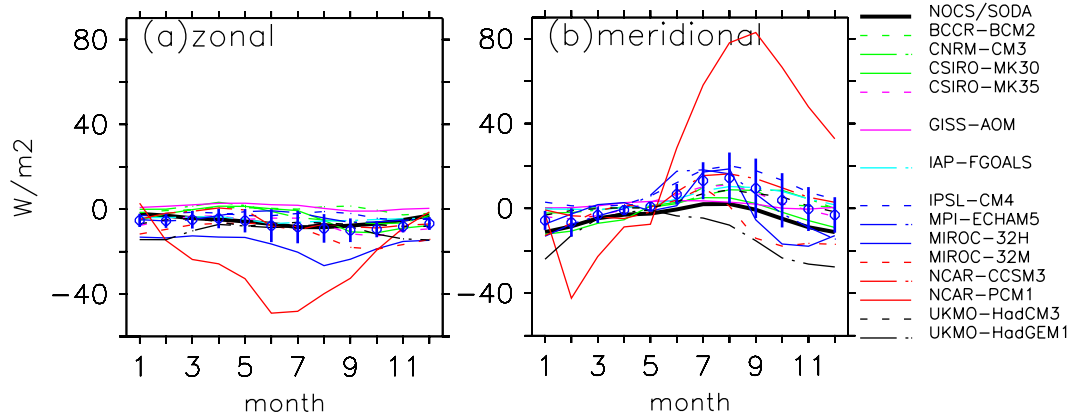
Fig. 6. The climatological seasonal variation in (a) zonal and (b) meridional advection for the upper 50 m of the ocean averaged for SODA and the 17 CMIP3 models in the south-central equatorial Pacific (units: W m^{-2}). The blue circles and blue vertical lines are the multi-model ensemble and uncertainties, respectively.

There are also some models that accurately simulate the advection, such as MIROC-32H, MIROC-32M and UKMO-HadGEM1, although these models also simulate weak DIB.

5. Summary

In this study, the temperature biases were investigated in the upper 50 m of the south-central equatorial Pacific using 17 CMIP3 models and nine sets of corresponding AMIP results. The reasons for the biases in the annual mean and the amplitude of seasonal variation were also investigated. We found that most simulated annual SST values in the research region are higher than the annual mean in observations. More than half of the models simulate large SST amplitudes over the study domain. Using heat budget analysis, we found that strong shortwave radiation in atmospheric models leads to warm SST bias. Weak southward cold advection is also an important mechanism for maintaining the high SST. The analysis of the seasonal circulation of the heat budget terms showed that the large SST amplitudes are mainly caused by large surface shortwave radiation amplitudes. These characteristics are especially obvious in models with strong SST warm biases.

The models with lower SST values also underestimate precipitation, which can be considered with small DIB biases. These types of models include MIROC-32H, MIROC-32M and UKMO-HadGEM1. According to our heat budget analysis, the low SST values are mainly caused by strong cold zonal or meridional advection.

The analysis presented in this paper shows that the main factors that lead to annual mean SST and its seasonal variation biases are the strong shortwave radiation reaching the sea surface and its large amplitude. Improving the radiative process in atmospheric models is crucial for reducing the SST bias and further attenuating the DIB. So far, however, we cannot clarify which exact processes lead to the biases in the surface shortwave radiation in each model. Further analysis focusing on one specific model may be helpful to find out

whether this is a problem of parameterization, or vertical resolution, or both.

REFERENCES

Adler, R. F., and Coauthors, 2003: The version-2 global precipitation climatology project (GPCP) monthly precipitation analysis (1979–present). *J. Hydrometeor.*, **4**, 1147–1167.

Bellucci, A., S. Gualdi, and A. Navarra, 2010: The double-ITCZ syndrome in coupled general circulation models: The role of large-scale vertical circulation regimes. *J. Climate*, **23**, 1127–1145.

Carton, J. A., and B. S. Giese, 2008: A reanalysis of ocean climate using Simple Ocean Data Assimilation (SODA). *Mon. Wea. Rev.*, **136**, 2999–3017.

Collins, W. D., and Coauthors, 2006: The Community Climate System Model Version 3 (CCSM3). *J. Climate*, **19**, 2122–2143.

Delworth, T. L. and Coauthors, 2006: GFDL's CM2 global coupled climate models–Part 1: Formulation and simulation characteristics. *J. Climate*, **19**(5), 643–674.

de Szoeke, S. P., and S. P. Xie, 2008: The tropical eastern Pacific seasonal cycle: Assessment of errors and mechanisms in IPCC AR4 coupled ocean-atmosphere general circulation models. *J. Climate*, **21**, 2573–2590.

Gent, P. R., and Coauthors, 2011: The community climate system model version 4. *J. Climate*, **24**, 4973–4991.

Gordon, C., C. Cooper, C.A. Senior, H. T. Banks, J. M. Gregory, T. C. Johns, J. F. B. Mitchell, and R. A. Wood, 2000: The simulation of SST, sea ice extents and ocean heat transports in a version of the Hadley Centre coupled model without flux adjustments. *Climate Dyn.*, **16**, 147–168.

Gordon, H. B., and Coauthors, 2002: The CSIRO Mk3 Climate System Model. CSIRO Atmospheric Research technical paper, No. 60, 130 pp.

Grist, J. P., and S. A. Josey, 2003: Inverse analysis adjustment of the SOC air-sea flux climatology using ocean heat transport constraints. *J. Climate*, **16**, 3274–3295.

Gualdi, S., E. Scoccimarro, and A. Navarra, 2008: Changes in tropical cyclone activity due to global warming: Results from a high-resolution coupled general circulation model. *J. Climate*, **21**, 5204-5228.

Gulev, S., T. Jung, and E. Ruprecht, 2007: Estimation of the impact of sampling errors in the VOS observations on air–sea fluxes. Part I. Uncertainties in climate means. *J. Climate*, **20**, 279–301.

Hasumi H., and S. Emori, 2004: K-1 coupled model (MIROC) description, K-1 technical report 1, Center for Climate System Research, University of Tokyo, 34pp. [Available online at http://www.ccsr.u-tokyo.ac.jp/kyosei/hasumi/MIROC/tech-repo.pdf.]

Johns, T. C., and Coauthors, 2006, The new Hadley Centre climate model HadGEM1: Evaluation of coupled simulations. *J. Climate*, **19**, 1327-1353.

Jungclaus, J.H., and Coauthors, 2006: Ocean circulation and tropical variability in the AOGCM ECHAM5/MPI-OM. *J. Climate*, **19**, 3952–3972.

Kent, E. C., and D. I. Berry, 2005: Quantifying random measurement errors in voluntary observing ships' meteorological observations. *Int. J. Climatol.*, **25**, 843–856, doi: 10.1002/joc.1167.

Large, W. G., and S. G. Yeager, 2008: The global climatology of an interannually varying air–sea flux data set. *Climate Dyn.*, **24**, 341–364, doi: 10.1007/s00382-008-0441–3.

Lee, T., I. Fukumori, and B. Y. Tang, 2004: Temperature advection: Internal versus external processes. *J. Phys. Oceanogr.*, **34**, 1936–1944.

Li, J. L., X. H. Zhang, Y. Q. Yu, and F. S. Dai, 2003: Double ITCZ phenomenon and analysis of its heat budget in a coupled ocean-atmosphere general circulation model. *Acta Meteorologica Sinica*, **61**, 39–51. (in Chinese)

Lin, J. L., 2007: The double-ITCZ problem in IPCC AR4 coupled GCMS: ocean-atmosphere feedback analysis. *J. Climate*, **20**(18), 4497–4525.

Liu, H. L., W. Y. Lin, and M. H. Zhang, 2010: Heat budget of the upper ocean in the south-central equatorial Pacific. *J. Climate*, **23**(7), 1779–1792.

Liu, H. L., M. H. Zhang, and W. Y. Lin, 2012: An Investigation of the Initial Development of the Double-ITCZ Warm SST Biases in the CCSM. *J. Climate*, **25**(1), 140–155.

Ma, C. C., C. R. Mechoso, A. W. Robertson, and A. Arakawa, 1996: Peruvian stratus clouds and the tropical Pacific circulation: A coupled ocean-atmosphere GCM study. *J. Climate*, **9**, 1635–1645.

Marti, O., and Coauthors, 2005: The new IPSL climate system model: IPSL-CM4, Note du Pôle de Modêlisation, *IPSL*, **26**, 1–86.

Mechoso, C. R., and Coauthors, 1995: The seasonal cycle over the tropical Pacific in coupled ocean-atmosphere general circulation models. *Mon. Wea. Rev.*, **123**, 3825–3838.

Meehl, G. A., W. M. Washington, C. Ammann, J. M. Arblaster, T. M. L. Wigley, and C. Tebaldi, 2004: Combinations of natural and anthropogenic forcings and 20th century climate. *J. Climate*, **17**, 3721–3727.

Rosati, A., and K. Miyakoda, 1988: A general circulation model for upper ocean simulation. *J. Phys. Oceanogr.*, **18**, 1601–1626.

Russell, G. L., J. R. Miller, and D. Rind, 1995: A coupled atmosphere-ocean model for transient climate change studies. *Atmos.–Ocean*, **33**(4), 683–730.

Salas-Mélia D., and Coauthors, 2005: Description and validation of the CNRM-CM3 global coupled model. CNRM working note 103, 36 pp.

Song, X. Z., and L. S. Yu, 2012: High-latitude contribution to global variability of air–sea sensible heat flux. *J. Climate*, **25**(10), 3515–3531. doi: 10.1175/JCLI-D-11-00028.1.

Schmidt, G. A., and Coauthors, 2006: Present day atmospheric simulations using GISS ModelE: Comparison to in-situ, satellite and reanalysis data. *J. Climate*, **19**, 153–192.

Xu, Y., Z. C. Zhao, Y. Luo, and X. J. Gao，2005: Climate change projections for the 21st century by the NCC/IAP T63 model with SRES scenarios. *Acta Meteorologica Sinica*, **19**, 407–417.

Yu, L. S., 2007: Global variations in oceanic evaporation (1958–2005): The role of the changing wind speed. *J. Climate*, **20**, 5376–5390, doi: 10.1175/2007JCLI1714.1.

Yu, L. S., and R. A. Weller, 2007: Objectively analyzed air–sea heat fluxes for the global ice-free oceans (1981–2005). *Bull. Amer. Meteor. Soc.*, **88**(4), 527–539, doi: 10.1175/BAMS-88–4-527.

Yu, Y. Q., X. H. Zhang, and Y. F. Guo, 2004: Global coupled ocean-atmosphere general circulation models in LASG/IAP. *Adv. Atmos. Sci.*, **21**, 444–455.

Zhang, G. J., and X. L. Song, 2010: Convection parameterization, tropical Pacific double ITCZ, and upper-ocean biases in the NCAR CCSM3. Part II: Coupled feedback and the role of ocean heat transport. *J. Climate*, **23**, 800–812.

Zhang, X. H., W. Y. Lin, and M. H. Zhang, 2007: Toward understanding the double Intertropical Convergence Zone pathology in coupled ocean-atmosphere general circulation models. *J. Geophys. Res.*, **112**(D12), doi: 10.1029/2006JD007878.

Zhang, Y. C., W. B. Rossow, A. A. Lacis, V. Oinas, and M. I. Mishchenko, 2004: Calculation of radiative fluxes from the surface to top of atmosphere based on ISCCP and other global data sets: Refinements of the radiative transfer model and the input data. *J. Geophys. Res.*, **109**, D19105, doi: 10.1029/2003JD004457.

Zheng, Y. X., T. Shinoda, J. L. Lin, and G. N. Kiladis, 2011: Sea surface temperature biases under the stratus cloud deck in the southeast Pacific Ocean in 19 IPCC AR4 coupled general circulation models. *J. Climate*, **24**(15), 4139–4164.